Single-Molecule Magnets: Site-Specific Ligand Abstraction from $[Mn_{12}O_{12}(O_2CR)_{16}(H_2O)_4]$ and the Preparation and Properties of $[Mn_{12}O_{12}(NO_3)_4(O_2CCH_2Bu^t)_{12}(H_2O)_4]$

Pau Artus,[†] Colette Boskovic,[†] Jae Yoo,[‡] William E. Streib,[†] Louis-Claude Brunel,[§] David N. Hendrickson,*[,‡] and George Christou*[,†]

Department of Chemistry and Molecular Structure Center, Indiana University, Bloomington, Indiana 47405-7102, Department of Chemistry-0358, University of California at San Diego, La Jolla, California 92093-0358, and Center for Interdisciplinary Magnetic Resonance, National High Magnetic Field Laboratory, Florida State University, Tallahassee, Florida 32310

Received March 6, 2001

Site-selective carboxylate abstraction has been achieved from $[Mn_{12}O_{12}(O_2CR)_{16}(H_2O)_4]$ complexes by treatment with HNO_3 in MeCN. The reaction of the R = Ph or CH_2Bu^t complexes with 4 equiv of HNO_3 gives $[Mn_{12}O_{12}(NO_3)_4(O_2CR)_{12}(H_2O)_4]$ (R = CH_2Bu^t (**6**) or Ph (**7**)) in analytical purity. Complex **6**·$MeNO_2$ crystallizes in monoclinic space group *C*2/*c* with the following cell parameters at −168 °C: $a = 21.280(5)$, $b = 34.430(8)$, $c = 33.023(8)$ Å, $\beta = 104.61(1)°$, $V = 23413$ Å, and $Z = 8$. The four NO_3^- groups are not disordered and are bound in bridging modes at axial positions formerly occupied by bridging carboxylate groups. ^1H NMR spectroscopy in CD_2Cl_2 and $CDCl_3$ shows retention of the solid-state structure on dissolution in these solvents. DC magnetic susceptibility (χ_M) and magnetization (M) studies have been carried out in the 2.00−300 K and 1.0−7.0 T ranges. Fits of $M/N\mu_B$ versus H/T plots gave S = 10, $g = 1.92$, and $D = -0.40$ cm^{-1}, where D is the axial zero-field splitting parameter. AC magnetic susceptibility studies on **6** have been performed in the 1.70−10.0 K range in a 3.5 Oe field oscillating at frequencies up to 1500 Hz. Out-of-phase magnetic susceptibility (χ_M'') signals were observed in the 4.00−8.00 K range which were frequency-dependent. Thus, **6** displays the slow magnetization relaxation diagnostic of a single-molecule magnet (SMM). The data were fit to the Arrhenius law, and this gave the effective barrier to relaxation (U_{eff}) of 50.0 cm^{-1} (72.0 K) and a pre-exponential ($1/\tau_0$) of 1.9×10^8 s^{-1}. Complex **6** also shows hysteresis in magnetization versus DC field scans, and the hysteresis loops show steps at regular intervals of magnetic field, the diagnostic evidence of field-tuned quantum tunneling of magnetization. High-frequency EPR (HFEPR) spectroscopy on oriented crystals of complex **6** shows resonances assigned to transitions between zero-field split M_s states of the S = 10 ground state. Fitting of the data gave S = 10, $g = 1.99$, $D = -0.46$ cm^{-1}, and $B_4^0 = -2.0 \times 10^{-5}$, where B_4^0 is the quartic zero-field coefficient. The combined results demonstrate that replacement of four carboxylate groups with NO_3^- groups leads to insignificant perturbation of the magnetic properties of the Mn_{12} complex. Complex **6** should now be a useful starting point for further reactivity studies, taking advantage of the good leaving group properties of the NO_3^- ligands.

Introduction

Since it was discovered in 1993 that single molecules of $[Mn_{12}O_{12}(O_2CMe)_{16}(H_2O)_4]$ (**1**) are superparamagnets and thus can act as magnets at very low temperatures,[1,2] there has been great interest in trying to understand this new magnetic phenomenon of single-molecule magnetism and in finding other compounds that exhibit similar properties. Since then, a few more manganese,[3−6] vanadium,[7] and iron[8] clusters have been found to possess the necessary properties to function as single-molecule magnets (SMM's). However, of the SMM's known to date, the $[Mn_{12}O_{12}(O_2CR)_{16}(H_2O)_4]$ (R = various) family possesses the best structural and electronic properties for this phenomenon inasmuch as it displays single-molecule magnetism behavior at the highest temperatures.

* To whom correspondence should be addressed.
† Indiana University.
‡ University of California at San Diego.
§ Florida State University.

(1) Sessoli, R.; Tsai, H.-L.; Schake, A. R.; Wang, S.; Vincent, J. B.; Folting, K.; Gatteschi, D.; Christou, G, Hendrickson, D. N. *J. Am. Chem. Soc.* **1993**, *115*, 1804.
(2) Sessoli, R.; Gatteschi, D.; Caneschi, A.; Novak, M. A. *Nature* **1993**, *365*, 141.
(3) (a) Tsai, H.-L.; Eppley, H. J.; de Vries, N.; Folting, K.; Christou, G.; Hendrickson, D. N. *Chem. Commun.* **1994**, 1745. (b) Eppley, H. J.; Esai, H.-L.; de Vries, N.; Folting, K.; Christou, G.; Hendrickson, D. N. *J. Am. Chem. Soc.* **1995**, *117*, 301.
(4) (a) Aubin, S. M. JU.; Wemple, M. W.; Adams, D. M.; Tsai, H.-L.; Christou, G.; Hendrickson, D. N. *J. Am. Chem. Soc.* **1996**, *118*, 7746. (b) Aubin, S. M. J.; Dilley, N. R.; Wemple, M. W.; Maple, M. B.; Christou, G.; Hendrickson, D. N. *J. Am. Chem. Soc.* **1998**, *120*, 839. (c) Aubin, S. M. J.; Dilley, N. R.; Pardi, L.; Krzystek, J.; Wemple, M. W.; Brunel, L.-C.; Maple, M. B.; Christou, G.; Hendrickson, D. N. *J. Am. Chem. Soc.* **1998**, *120*, 4991.
(5) (a) Aubin, S. M. J.; Sun, Z.; Guzei, I. A.; Rheingold, A. L.; Christou, G.; Hendrickson, D. N. *Chem. Commun.* **1997**, 2239. (b) Sun, Z.; Ruiz, D.; Rumberger, E.; Incarvito, C. D.; Folting, K.; Rheingold, A. L.; Christou, G.; Hendrickson, D. N. *Inorg. Chem.* **1998**, *37*, 4758.
(6) (a) Brechin, E. K.; Yoo, J.; Nakano, M.; Huffman, J. C.; Hendrickson, D. N.; Christou, G. *Chem. Commun.* **1999**, 783. (b) Yoo, J.; Brechin, E. K.; Yamaguchi, A.; Nakano, M.; Huffman, J. C.; Maniero, A. L.; Brunel, L.-C.; Awaga, K.; Ishimoto, H.; Christou, G.; Hendrickson, D. N. *Inorg. Chem.* **2000**, *39*, 3615.
(7) Castro, S. L.; Sun, Z.; Grant, C. M.; Bollinger, J. C.; Hendrickson, D. N.; Christou, G. *J. Am. Chem. Soc.* **1998**, *120*, 2365.
(8) (a) Sangregorio, C.; Ohm, T.; Paulsen, C.; Sessoli, R.; Gatteschi, D. *Phys. Rev. Lett.* **1997**, *78*, 4645. (b) Oshio, H.; Hoshino, N.; Ito, T. *J. Am. Chem. Soc.* **2000**, *122*, 12602. (c) Barra, A.-L.; Caneschi, A.; Cornia, A.; Fabrizi de Biani, F.; Gatteschi, D.; Sangregorio, C.; Sessoli, R.; Sorace, L. *J. Am. Chem. Soc.* **1999**, *121*, 5302.

10.1021/ic010252g CCC: $20.00
Published on Web 07/06/2001

The study of the physics of nanoscale magnetic particles has particularly benefited from the discovery of SMM's since the latter represented, for the first time, the availability of a collection of magnetic "particles" with a single, sharply defined size, i.e., the molecular size. This allowed for the observation of quantum effects that had been predicted[9−11] but never before clearly seen, such as quantum tunneling of the magnetization (QTM).[12,13] This fact has triggered the expansion of this field and contributed to the understanding of the consequences of taking magnetic materials to the limit of miniaturization, where quantum effects have to be taken into account.

After it was understood that a large ground state spin (S) and a magnetic anisotropy with a negative value of the ZFS parameter *D* (i.e., easy axis type anisotropy) are the key to this behavior, a new effort began in trying to modify these molecules in a controlled fashion. This has been successful and has allowed the study of the effects of various modifications on the resulting magnetic properties, giving a better understanding of the structural and electronic factors that directly influence the latter. Work within the area of Mn_{12} coordination chemistry has led to the development of methods for altering the chemical environment of the Mn_{12} core. It is, for example, possible to exchange the $MeCO_2^-$ ligands of the $[Mn_{12}O_{12}(O_2CMe)_{16}(H_2O)_4]$ complex for almost any type of organic carboxylate group.[3b] This represented a big step forward because, among other things, it increased the solubility properties of these clusters in organic solvents and greatly altered their redox potentials, significantly expanding the chemistry of this family of molecules.[3b] One of the first results derived from the latter was the synthesis and isolation of the one-electron reduced species, $[Mn_{12}O_{12}(O_2CR)_{16}(H_2O)_4]^-$, which allowed for the study of the SMM phenomenon on a half-integer spin system.[3,14,15] More recently, the two-electron reduced species have also been isolated and studied.[16]

Among the many lines currently being pursued by our group in this field is the introduction of new types of ligands (i.e., other than organic carboxylate groups); this is of great interest because it might more greatly modify the electronic properties of the cluster and could thus significantly affect the magnetic behavior. Also, looking toward future applications, it would be desirable to be able to chemically bind the complex to other species, such as surfaces or even macromolecules, without loss of the magnetic properties of the Mn_{12} species, and this would become feasible if controllable alteration of peripheral ligands, in other words, controlled functionalization of the molecule, could be achieved. In this paper, we report some new progress along these lines. The site-specific replacement of four of the carboxylate groups on $[Mn_{12}O_{12}(O_2CR)_{16}(H_2O)_4]$ with NO_3^- groups has been achieved, and the structure and properties of the resulting product are described, including the results of a magnetochemical study that confirms that these new derivatives of the Mn_{12} family retain single-molecule magnetism properties.

Experimental Section

All manipulations were performed under aerobic conditions using materials as received, except where otherwise noted. $[Mn_{12}O_{12}(O_2CMe)_{16}(H_2O)_4]$ (**1**), $[Mn_{12}O_{12}(O_2CEt)_{16}(H_2O)_3]$ (**2**), $[Mn_{12}O_{12}(O_2CCH_2Bu^t)_{16}(H_2O)_4]$ (**3**), and $[Mn_{12}O_{12}(O_2CPh)_{16}(H_2O)_4]$ (**4**) were prepared using the ligand substitution procedure as described.[3b] A stock solution of 0.226 M HNO_3 in MeCN was prepared by adding 70% HNO_3 (0.509 g, 5.65 mmol) to MeCN and making up the volume to 25.0 mL. A 0.48 M stock solution was prepared similarly using 1.08 g (12.0 mmol) of 70% HNO_3.

$[Mn_{12}O_{12}(NO_3)_x(O_2CMe)_{16-x}(H_2O)_4]$ (5; x ≈ 3.5). A solution of complex **1**·$4H_2O.2MeCO_2H$ (1.0 g, 0.49 mmol) in MeCN (100 mL) was treated with a solution of HNO_3 (0.48 M, 4.55 mL, 2.18 mmol). After a few minutes, the solution was filtered, and the filtrate was maintained undisturbed for two weeks at room temperature in a sealed flask. The resultant microcrystalline solid was collected by filtration, washed with Et_2O, and dried in vacuo. The yield was 0.65 (68%). Anal. Calcd (found) for **5**·$5H_2O$ with $x = 3.5$: C, 15.25 (14.87); H, 2.84 (2.89); N, 2.49 (2.18).

$[Mn_{12}O_{12}(NO_3)_4(O_2CCH_2Bu^t)_{12}(H_2O)_4]$ (6). A solution of complex **3** (0.500 g, 0.181 mmol) in CH_2Cl_2 (25 mL) was treated with a solution of HNO_3 (0.226 M, 3.60 mL, 0.814 mmol). No noticeable color change occurred. After 1 h, $MeNO_2$ (10 mL) was added, the solution was filtered, and the filtrate was allowed to concentrate by evaporation of the CH_2Cl_2 for 1 to 2 days. The resultant solid was collected by filtration, washed with hexanes, and dried in vacuo. The yield was 0.41 g (88%). Anal. Calcd (found) for **6**·$^1/_2Bu^tCH_2CO_2H$: C, 34.50 (34.43); H, 5.64 (5.56); N, 2.15 (2.23). Washing with $MeNO_2$ and drying of the solid leads to complete loss of the $Bu^tCH_2CO_2H$. Anal. Calcd (found) for **6**·H_2O: C, 33.63 (33.64); H, 5.57 (5.73); N, 2.18 (2.20). X-ray quality crystals of **6**·$MeNO_2$ were grown by slow evaporation of a solution of the complex in $MeNO_2/CH_2Cl_2$ (1:1).

$[Mn_{12}O_{12}(NO_3)_4(O_2CPh)_{12}(H_2O)_4]$ (7). A solution of complex **4** (0.25 g, 0.084 mmol) in CH_2Cl_2 (25 mL) was treated with a solution of HNO_3 (0.48 M, 0.71 mL, 0.336 mmol), and the mixture stirred while a precipitate was forming. When precipitation appeared to be complete, the solid was collected by filtration, washed with hexanes, and dried in vacuo. The yield was 0.16 g (72%). Anal. Calcd (found) for **7**·$3H_2O$: C, 37.66 (37.92); H, 2.78 (2.77); N, 2.09 (1.76).

Conversion of Complex 6 to Complex 3. To a solution of complex **6** (0.1 g, 0.04 mmol) in CH_2Cl_2 (15 mL) was added a solution of $NaO_2CCH_2Bu^t$ (0.024 g, 0.17 mmol) in MeOH (1 mL), and the mixture was stirred for 1 h. The dark brown solution was filtered to remove some white solid ($NaNO_3$), and the solvent was removed from the filtrate under vacuum. The solid residue was dissolved in a mixture of $CH_2Cl_2/MeNO_2$ (10 mL, 1:1 v/v), filtered, and the filtrate allowed to concentrate by evaporation for 2 days, during which time a black crystalline solid appeared. This was collected by filtration, washed with a little $MeNO_2$, and dried in air. Yield, 0.051 g (46%). Anal. Calcd (found) for **3**·$2MeNO_2$: C, 41.25 (41.03); H, 6.58 (6.83); N, 0.96 (0.96).

X-ray Crystallography and Structure Solution. Data were collected on a Picker four-circle diffractometer at −168 °C; details of the diffractometry, low-temperature facilities, and computational procedures employed by the Molecular Structure Center are available elsewhere.[17] Small black crystals of **6**·$MeNO_2$ suitable for X-ray diffraction were selected from the bulk samples and transferred to the goniostat, where they were cooled to −168 °C for characterization and data collection ($6° \le 2\theta \le 45°$, $+h, +k, \pm l$). A preliminary search for peaks followed by analysis using programs DIRAX and TRACER revealed a *C*-centered monoclinic cell. Following intensity data collection, the additional condition $l = 2n$ for $h01$ limited the space group to *Cc* or *C*2/*c*. The choice of *C*2/*c* was later proven to be correct by the successful solution of the structure. After an analytical correction for absorption, data processing gave a unique set of 15362 intensities and an $R_{av} = 0.046$ for the averaging of 2090 of these that had been measured more than once. Four standards collected every 300 data showed no significant trends.

(9) Chudnovsky, E. M.; Gunter, L. *Phys. Rev. Lett.* **1988**, *60*, 661.
(10) Enz, M.; Schilling, R. *J. Phys. C: Solid State Phys.* **1986**, *19*, 1765.
(11) van Hemmen, J. L.; Suto, A. *Europhys. Lett.* **1986**, *1*, 481.
(12) Friedman, J. R.; Sarachik, M. P.; Tejada, J.; Ziolo, R. *Phys. Rev. Lett.* **1996**, *76*, 3830.
(13) (a) Thomas, L.; Lionti, F.; Ballou, R.; Gatteschi, D.; Sessoli, R.; Barbara, B. *Nature* **1996**, *383*, 145. (b) Tejada, J.; Ziolo, R. F.; Zhang, X. X. *Chem. Mater.* **1996**, *8*, 1784.
(14) Aubin, S. M. J.; Spagna, S.; Eppley, H. J.; Sager, R. E.; Christou, G.; Hendrickson, D. N. *Chem. Commun.* **1998**, 803.
(15) Aubin, S. M. J.; Sun, Z.; Pardi, L.; Krzystek, J.; Folting, K.; Brunel, L.-C.; Rheingold, A. L.; Christou, G.; Hendrickson, D. N. *Inorg. Chem.* **1999**, *38*, 5329.
(16) Soler, M.; Chandra, S. K.; Ruiz, D.; Davidson, E. R.; Hendrickson, D. N.; Christou, G. *Chem. Commun.* **2000**, 2417.
(17) Chisholm, M. H.; Folting, K.; Huffman, J. C.; Kirkpatrick. C. C. *Inorg. Chem.* **1984**, *23*, 1021.

Table 1. Crystallographic Data for $[Mn_{12}O_{12}(NO_3)_4(O_2CCH_2Bu^t)_{12}(H_2O)_4]\cdot MeNO_2$ (**6**·$MeNO_2$)

formula	$C_{73}H_{143}Mn_{12}N_5O_{54}$[a]	space group	*C*2/*c*
a, Å	21.280(5)	*T*, °C	−168
b, Å	34.430(8)	*λ*, Å	0.71069[b]
c, Å	33.023(8)	ρ_{calc}, g/cm^{-3}	1.483
β, °	104.61(1)	μ(Mo K$_a$), cm^{-1}	13.330
V, Å^3	23413	*R*	0.0746[c]
Z	8	R_w	0.0754[c]
FW, g mol^{-1}	2614.20		

[a] Including solvate molecules. [b] Graphite monochromator. [c] $R = \sum||F_o| - |F_c||/\sum|F_o|$ and $R_w = [\sum w(|F_o| - |F_c|)^2/\sum w|F_o|^2]^{1/2}$ where $w = 1/\sigma^2(|F_o|)$.

The structure was solved using a combination of direct methods (MULTAN78) and Fourier techniques. All non-hydrogen atoms were readily located. Hydrogen atoms bonded to carbon atoms were included in fixed, calculated positions, with thermal parameters fixed at one plus the isotropic thermal parameter of the parent carbon atom. Hydrogen atoms on the water ligands could not be calculated unambiguously; they were not observed in the difference Fourier maps and, therefore, were not included in the refinements. In the final cycles of refinement, 11 atoms in terminal groups that had not converged properly to the anisotropic form were varied with isotropic thermal parameters. The other 133 non-hydrogen atoms were varied with anisotropic thermal parameters, which, with a scale and extinction parameter, gave a total of 1243 variables. Data with $I < 2\sigma(I)$ were considered unobserved. The final $R(F) = 0.075$ for the observed data and 0.131 for all data, and $R_w(F) = 0.075$ for the observed data and 0.082 for all data. The final difference Fourier map was reasonably clean, the largest peak being 1.03 e/Å^3 and the deepest hole being −0.86 e/Å^3. Crystallographic data are listed in Table 1.

Other Studies. Infrared spectra were recorded on KBr pellets using a Nicolet 510P FTIR spectrophotometer. ^{1}H NMR spectra were obtained with a Varian XL-300 spectrometer; chemical shifts are quoted using the *δ* scale (shifts downfield are positive). Variable-temperature magnetic susceptibility data were obtained with a Quantum Design MPMS5 SQUID susceptometer, at University of California San Diego, or a MPMSXL SQUID susceptometer, at Indiana University, equipped with a 5.5 or 7 T magnet, respectively. Pascal's constants were used to estimate the diamagnetic correction, which was subtracted from the experimental susceptibility to give the molar magnetic susceptibility (χ_M).

High-frequency EPR spectra were recorded at the National High Magnetic Field Laboratory, Tallahassee, Florida. The spectrometer is equipped with a 14.5 T superconducting magnet and can achieve temperatures ranging from 4 to 300 K. A Gunn diode operating at a fundamental frequency of 110 ± 3 GHz was used. The operating frequency range is 110−550 GHz. Frequencies between 220 and 550 GHz were obtained by using a solid-state harmonic generator that multiplies the fundamental frequency (i.e., 110 GHZ) and uses high pass filters to filter out the lower frequency harmonics; however, the higher frequency harmonics pass through. A modulation frequency of 8.5 kHz was used for phase-sensitive detection. The magnetic field was swept at a rate of 0.2 T/min over a 0−14.5 T range.

Results and Discussion

Syntheses. The $[Mn_{12}O_{12}(O_2CR)_{16}(H_2O)_4]$ complexes are mixed-valent $8Mn^{III}$, $4Mn^{IV}$ and contain a central $[Mn^{IV}_4O_4]$ cubane held within a nonplanar ring of eight Mn^{III} ions by eight μ_3-O^{2-} ions (Figure 1). Peripheral ligation is by sixteen μ-RCO_2^- and four terminal H_2O groups. The complete molecule has virtual D_2 or S_4 symmetry (depending on the relative disposition of the H_2O molecules and certain RCO_2^- groups, i.e., geometric isomers are possible) and thus the carboxylate groups separate into four types by symmetry. Therefore, site-specific carboxylate abstraction from a multinuclear metal cluster such as $[Mn_{12}O_{12}(O_2CR)_{16}(H_2O)_4]$ that contains a number of inequivalent carboxylate groups requires a significant degree of kinetic or thermodynamic differentiation of one type of carboxylate group from the rest. Such a differentiation exists in the $[Mn_{12}O_{12}(O_2CR)_{16}(H_2O)_4]$ clusters, and it arises from the presence of a Jahn−Teller (JT) distortion at each of the eight near-octahedral high-spin Mn^{III} ions (d^4, $S = 2$), which takes the form of an axial elongation of two trans bonds. This structural effect has important consequences on the relative reactivity of the carboxylate groups for the following reasons. First, a JT elongation of a metal−ligand bond will weaken that bond. For a donor ligand such as a carboxylate, this will serve to maintain a greater electron density on the O atoms compared with the O atoms of Mn−O bonds not JT elongated. This will make RCO_2^- groups possessing an O atom lying on a JT axis more susceptible to electrophilic attack at the O atom, and this could form the basis for selective abstraction of these RCO_2^- groups. Second, the RCO_2^- groups in $[Mn_{12}O_{12}(O_2CR)_{16}(H_2O)_4]$ clusters are all bridging, with each O atom attached to a different Mn ion; thus, even those RCO_2^- groups lying on JT axes fall into two types, those with only one of their O atoms on a JT axis, and those with both their O atoms lying on JT axes. In Figure 1, a representative $[Mn_{12}O_{48}]$ core of a $[Mn_{12}O_{12}(O_2CR)_{16}(H_2O)_4]$ complex is shown; this belongs to the R = C_6H_4-*p*-Me complex described elsewhere,[23] but will serve as a typical example for the present discussion. The core is approximately disk-shaped, and the eight Mn^{III} elongation axes (solid black bonds) are seen to all be axial with respect to the plane of the molecule. There are a total of sixteen O atoms lying on the eight JT axes, they partition into the following groups: (a) four O atoms from four H_2O molecules, (b) four O atoms from four RCO_2^- groups whose other O atom is attached to a Mn^{IV} ion in the central cube, and (c) eight O atoms from four RCO_2^- groups bridging Mn^{III} ions. Thus, each

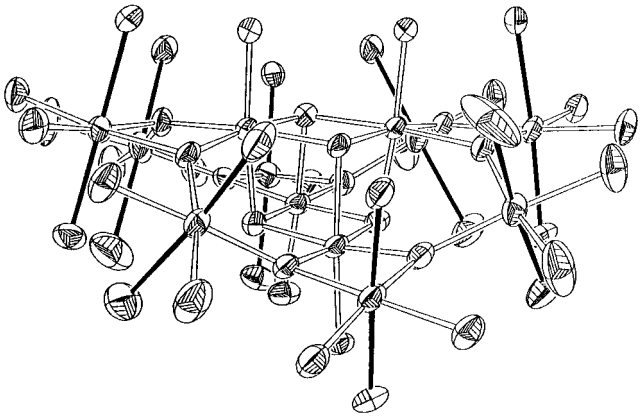

Figure 1. The $[Mn_{12}O_{48}]$ core of a typical $[Mn_{12}O_{12}(O_2CR)_{16}(H_2O)_4]$ complex showing the relative disposition of the Jahn−Teller elongation axes indicated as solid black bonds.

(18) (a) Libby, E.; McCusker, J. K.; Schmitt, E. A.; Folting, K.; Hendrickson, D. N.; Christou, G. *Inorg. Chem.* **1991**, *30*, 3486. (b) Libby, E.; Folting, K.; Huffman, C. J.; Huffman, J. C.; Christou, G. *Inorg. Chem.* **1993**, *32*, 2549.
(19) Artus, P.; Christou, G., manuscript in preparation.
(20) Nakamoto, K. *Infrared and Raman Spectra of Inorganic and Coordination Compounds*, 4th ed.; Wiley-Interscience: New York, 1986.
(21) Vincent, J. B.; Christmas, C.; Chang, H.-R.; Li, Q.; Boyd, P. D. W.; Huffman, J. C.; Hendrickson, D. N.; Christou, G. *J. Am. Chem. Soc.* **1989**, *111*, 2086.
(22) Sun, Z.; Ruiz, D.; Dilley, N. R.; Soler, M.; Ribas, J.; Folting, K.; Maple, M. B.; Christou, G.; Hendrickson, D. N. *Chem. Commun.* **1999**, 1973.
(23) Aubin, S. M. J.; Sun, Z.; Eppley, H. J.; Rumbergber, E.; Guzei, I. A.; Folting, K.; Gantzel, P. K.; Rheingold, A. L.; Christou, G.; Hendrickson, D. G. *Inorg. Chem.*, in press.

RCO_2^- group of type (c) has both of its O atoms lying on JT axes, and it was suspected that this might form the basis for the selective abstraction of these four RCO_2^- with a suitably chosen electrophilic reagent. There existed precedent for believing this. The complex $[Mn_4O_2(O_2CR)_7(pic)_2]^-$ (pic^- = picolinate)[18a] has one unique RCO_2^- group that has both O atoms on JT elongation axes, whereas the other six have only one O on a JT axis. It was found[18] that (i) the unique RCO_2^- group is more labile, undergoing more rapid substitution with free RCO_2H in solution, and (ii) this RCO_2^- group can be selectively removed by electrophilic attack by stoichiometric Me_3SiCl to give the silyl ester (eq 1), producing either $[Mn_4O_2(O_2CPh)_6(MeCN)_2(pic)_2]$ or dimeric $[Mn_4O_2(O_2CMe)_6(pic)_2]_2$, depending on the R group.[18]

$$[Mn_4O_2(O_2CR)_7(pic)_2]^- + Me_3SiCl \xrightarrow[MeCN]{} \text{“}[Mn_4O_2(O_2CR)_6(pic)_2]\text{”} + Me_3SiO_2CR + Cl^- \quad (1)$$

Another observation also indicates that four RCO_2^- groups in the Mn_{12} complexes might be selectively abstractable; in VT NMR studies it has been discovered[19] that there is a fluxional process involving these μ-RCO_2^- groups exchanging position with a neighboring H_2O group, as shown. This reversible conversion of these RCO_2^- groups from a μ- to a terminal binding mode also supports the feasibility of selective abstraction via their enhanced reactivity with electrophiles while in a monodentate mode. Thus, such reactions were investigated in detail.

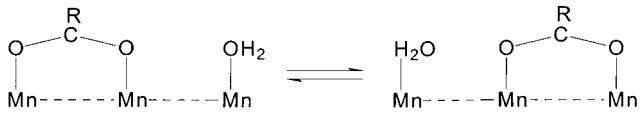

Preliminary studies using Me_3SiCl proved to be unsuccessful, as defined by the isolation of any pure product; we suspect the problem is that the putative Cl^-/solvent product, e.g., “$[Mn_{12}O_{12}(O_2CR)_{12}Cl_4(MeCN)_4(H_2O)_4]$”, may be too unstable to the subsequent degradative reaction. Thus, reagents that also provide groups better able to occupy the formerly carboxylate sites were sought, and mineral acids were chosen. Both H_2SO_4 and H_3PO_4 gave unstable products as judged by precipitation of dark, insoluble precipitates, which are probably Mn oxides based on IR signatures in the 400−700 cm^{-1} range. However, the addition of four equivalents of HNO_3 to $[Mn_{12}O_{12}(O_2CMe)_{16}(H_2O)_4]$ (**1**) did not give a precipitate, and the product seemed indefinitely stable in solution. Microcrystals obtained from solvent evaporation gave IR and NMR data indicating a Mn_{12} product with decreased $MeCO_2^-$ content and the presence of NO_3^- groups. However, the elemental analysis data indicated there were <4 NO_3^- groups, suggesting that if the desired substitution had been achieved, it was not complete. Use of the propionate complex **2** also led to a product that could not be isolated in pure form. A number of other, more soluble $[Mn_{12}O_{12}(O_2CR)_{16}(H_2O)_4]$ complexes were then explored, with a concentration of effort on the R = Ph and CH_2Bu^t species, and these were found to give pure, isolable materials of formulation $[Mn_{12}O_{12}(NO_3)_4(O_2CR)_{12}(H_2O)_4]$. A subsequent crystal structure on the R = CH_2Bu^t complex **6** confirmed that site-selective substitution of four RCO_2^- groups had indeed occurred (vide infra). The formation of the product is summarized in eq 2.

$$[Mn_{12}O_{12}(O_2CR)_{16}(H_2O)_4] + 4\,HNO_3 \rightarrow [Mn_{12}O_{12}(NO_3)_4(O_2CR)_{12}(H_2O)_4] + 4\,RCO_2H \quad (2)$$

For the reaction with the R = CH_2Bu^t complex (**3**), ratios of HNO_3:Mn_{12} other than 4:1 were also explored, up to a 10:1 ratio, and for the reaction times normally explored (≤1 h, followed by 1 to 2 days crystallization time after $MeNO_2$ is added), only the 4:1 product crystallized from solution, as confirmed by IR comparisons and (for the 10:1 product) elemental analysis. This suggests the other RCO_2^- groups are not as susceptible to attack and/or the low solubility of **6** is causing its precipitation from equilibria containing other $[Mn_{12}O_{12}(NO_3)_x(O_2CR)_{16-x}(H_2O)_4]$ species. Ratios higher than 10:1 gave various degrees of decomposition and appearance of insoluble dark powders.

The carboxylate abstraction can be reversed; treatment of complex **6** with 4 equiv of $NaO_2CCH_2Bu^t$ in CH_2Cl_2/MeOH gave complex **3** (eq 3).

$$[Mn_{12}O_{12}(NO_3)_4(O_2CR)_{12}(H_2O)_4] + 4\,NaO_2CR \rightarrow [Mn_{12}O_{12}(O_2CR)_{16}(H_2O)_4] + 4\,NaNO_3 \quad (3)$$

This supports the feasibility of using complexes such as **6** and **7** for subsequent reactions centered at the NO_3^- positions, taking advantage of the good leaving properties of this group.

The successful formation of **6** from the use of HNO_3 contrasts dramatically with the formation of Mn oxides when H_2SO_4 and H_3PO_4 were employed. It is possible that the additional protons present in these di- and triprotic acids, respectively, leads to further reaction of bound HSO_4^- or $H_2PO_4^-$, leading to loss of additional RCO_2^- groups as RCO_2H and thus triggering aggregation of the remaining Mn_{12} fragment to Mn oxides.

Crystal Structure of Complex 6. An ORTEP representation and stereoview of complex **6** are provided in Figure 2.

Selected interatomic distances and angles for **6** are listed in Table 2.

Complex **6** crystallizes in monoclinic space group *C*2/*c*, with the molecule in a general position. The core has the same overall structure as $[Mn_{12}O_{12}(O_2CR)_{16}(H_2O)_4]$ complexes comprising a central $[Mn^{IV}_4O_4]$ cubane and an outer ring of eight Mn^{III} ions. Four μ-NO_3^- groups are bridging in a fashion analogous to the RCO_2^- groups. The eight Mn^{III} JT axes are axial to the $[Mn_{12}O_{12}]$ core (i.e., as in Figure 1). The H_2O molecules are two each on Mn(8) and Mn(12), four axial RCO_2^- groups bridge $Mn^{III}Mn^{IV}$ pairs, and the four NO_3^- groups bridge Mn^{III}_2 pairs, with both their O atoms on JT axes. Thus, the NO_3^- groups are indeed at the four positions suggested to be the most susceptible to replacement. Note that the NO_3^- groups are completely ordered (100% occupancy) at the four positions shown; the carboxylate Bu^t groups have been omitted for clarity in Figure 2, but were located in the crystal structure with 100% occupancy. The JT elongated Mn−O bonds (Mn−ONO_2 = 2.190(7)−2.267(6), Mn−OH_2 = 2.201(7)−2.262(7), Mn−OCOR = 2.139(6)−2.160(6) Å) reflect weaker Mn−NO_3 bonds compared with Mn−O_2CR bonds, as expected. The average lengths are Mn−OCOR (2.151) < Mn−ONO_2 (2.231) = Mn−OH_2 (2.231 Å). These values are all significantly longer than the equatorial Mn−OCOR bonds (1.912(7)−1.962(6) Å, average 1.938 Å), consistent with the ∼0.2 Å JT bond elongation for equivalent ligands. The 2 + 2 disposition of H_2O molecules gives the molecule virtual D_2 symmetry.

^{1}H NMR Spectroscopy. The nature and stability of complex **6** in solution was investigated using ^{1}H NMR spectroscopy in $CDCl_3$ and CD_2Cl_2. In Figure 3 are shown the spectra for

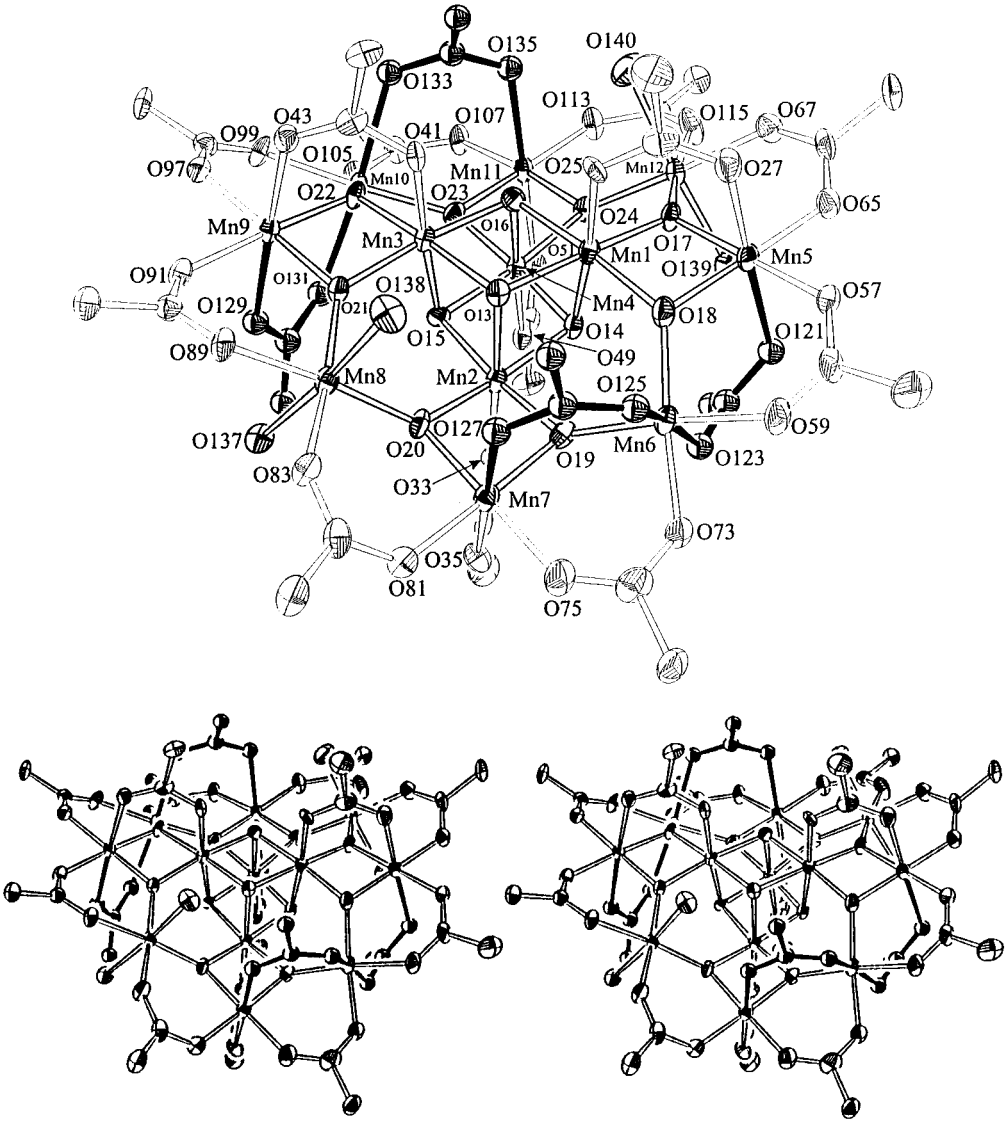

Figure 2. ORTEP plot and stereoview of $[Mn_{12}O_{12}(NO_3)_4(O_2CCH_2Bu^t)_{12}(H_2O)_4]$ (**6**) at the 50% probability level. For clarity, only the CH_2 carbon atom of each $Bu^tCH_2CO_2^-$ group is shown, and the positions of the NO_3^- groups are emphasized with solid black bonds.

complexes **3** and **6** in $CDCl_3$. The spectrum for **3** (Figure 3, top) shows four CH_2 resonances in a 1:1:1:1 integration ratio and three CH_3 resonances in an approximately 1:1:2 ratio. As described in more detail elsewhere, this spectrum is consistent with a molecule of effective D_{2d} solution symmetry, not D_2.[19] As mentioned above, there is a fluxional process involving exchange of the positions of a RCO_2^-/H_2O pair. At room temperature, this is fast on the ^1H NMR time scale and serves to introduce mirror planes perpendicular to the plane of the $[Mn_{12}O_{12}]$ disk. This makes the eight equatorial RCO_2^- groups equivalent, but the axial groups are still of two types. Therefore, the $Bu^tCH_2CO_2^-$ Me groups give three resonances in a 2:1:1 ratio. The CH_2 groups would also give the same 2:1:1 pattern except that the two CH_2 hydrogen atoms of the equatorial groups are diastereotopic, whereas those of the axial groups are equivalent (vertical mirror planes). Thus, a 1:1:1:1 pattern is observed.

If the solid-state structure of **6** is retained in solution, one type of axial carboxylate has been removed relative to **3**, and the spectrum should be correspondingly simpler. Indeed, Figure 3, bottom, shows that there are now only three CH_2 resonances in a 1:1:1 ratio and two Bu^t resonances in a 2:1 ratio, exactly as expected. The spectrum is otherwise clean and consistent with the NO_3^- groups occupying only the positions seen in the solid state. Note that the spectrum of **6** again indicates D_{2d} symmetry, i.e., a fluxional process involving NO_3^-/H_2O exchange is present. Variable-temperature studies for **3**, **6**, and many other Mn_{12} complexes will be reported elsewhere, where the fluxional process will be seen to be frozen out at low temperatures. The present data serve to show that complex **6** is stable in solution.

The chemical shifts in CD_2Cl_2 are collected in Table 3, which also includes the peak assignments. The Me (Bu^t) peaks are readily assignable, given the relative intensities and the disappearance of one peak that is therefore assigned to the axial groups bridging $Mn^{III}Mn^{III}$ pairs, which are replaced by NO_3^- groups. The resonance for the equatorial groups shifts only slightly (0.12 ppm) between **3** and **6**, whereas that for the axial groups shifts 0.38 ppm to $\delta = 2.76$ ppm. This probably reflects a greater sensitivity of these groups to the RCO_2^-/NO_3^- substitution, since the replaced group is trans to the axial RCO_2^- groups bridging $Mn^{III}Mn^{IV}$ pairs. This also allows for assignment of the CH_2 resonances; the very downfield resonance at 46.6 ppm is clearly from the substituted group, and the resonance at 18.0 ppm in **3** is assigned to the axial groups bridging $Mn^{III}Mn^{IV}$ since it shifts the most, to 22.6 ppm, in **6**. The

Table 2. Selected Interatomic Distances (Å) and Angles (Deg) for $[Mn_{12}O_{12}(NO_3)_4(O_2CCH_2Bu^t)_{12}(H_2O)_4]$ (**6**)

Mn(1)	Mn(2)		2.831(2)	Mn(2)	Mn(4)		2.948(2)
Mn(1)	Mn(3)		2.930(2)	Mn(2)	Mn(7)		2.782(2)
Mn(1)	Mn(4)		2.826(2)	Mn(3)	Mn(4)		2.820(2)
Mn(1)	Mn(5)		2.767(2)	Mn(3)	Mn(9)		2.758(2)
Mn(2)	Mn(3)		2.831(2)	Mn(4)	Mn(11)		2.795(2)
Mn(1)	Mn(12)		3.428(2)	Mn(3)	Mn(8)		3.423(2)
Mn(1)	Mn(6)		3.446(2)	Mn(3)	Mn(10)		3.440(2)
Mn(2)	Mn(6)		3.441(2)	Mn(4)	Mn(10)		3.425(2)
Mn(2)	Mn(8)		3.440(2)	Mn(4)	Mn(12)		3.427(2)
Mn(1)	O(13)		1.909(6)	Mn(9)	O(43)		2.160(6)
Mn(1)	O(14)		1.895(6)	Mn(9)	O(91)		1.922(6)
Mn(1)	O(16)		1.947(6)	Mn(9)	O(97)		1.934(7)
Mn(1)	O(17)		1.869(6)	Mn(9)	O(129)		2.267(6)
Mn(1)	O(18)		1.892(6)	Mn(10)	O(22)		1.873(6)
Mn(1)	O(25)		1.894(6)	Mn(10)	O(23)		1.874(6)
Mn(2)	O(13)		1.923(6)	Mn(10)	O(99)		1.945(6)
Mn(2)	O(14)		1.924(6)	Mn(10)	O(105)		1.944(6)
Mn(2)	O(15)		1.909(6)	Mn(10)	O(131)		2.216(7)
Mn(2)	O(19)		1.860(6)	Mn(10)	O(133)		2.216(7)
Mn(2)	O(20)		1.887(6)	Mn(11)	O(23)		1.895(6)
Mn(2)	O(33)		1.903(6)	Mn(11)	O(24)		1.911(6)
Mn(3)	O(13)		1.924(6)	Mn(11)	O(51)		2.139(6)
Mn(3)	O(15)		1.903(6)	Mn(11)	O(107)		1.946(6)
Mn(3)	O(16)		1.897(6)	Mn(11)	O(113)		1.923(7)
Mn(3)	O(21)		1.864(6)	Mn(11)	O(135)		2.256(7)
Mn(3)	O(22)		1.899(6)	Mn(12)	O(17)		1.866(6)
Mn(3)	O(41)		1.907(6)	Mn(12)	O(24)		1.884(6)
Mn(4)	O(14)		1.909(6)	Mn(12)	O(67)		1.936(7)
Mn(4)	O(15)		1.933(6)	Mn(7)	O(19)		1.875(6)
Mn(4)	O(16)		1.908(6)	Mn(7)	O(20)		1.892(6)
Mn(4)	O(23)		1.852(6)	Mn(7)	O(35)		2.156(7)
Mn(4)	O(24)		1.867(6)	Mn(7)	O(75)		1.932(7))
Mn(4)	O(49)		1.904(6)	Mn(7)	O(81)		1.942(7)
Mn(5)	O(17)		1.890(6)	Mn(7)	O(127)		2.225(7)
Mn(5)	O(18)		1.898(6)	Mn(8)	O(20)		1.900(6)
Mn(5)	O(27)		2.148(7)	Mn(8)	O(21)		1.883(6)
Mn(5)	O(57)		1.927(7)	Mn(8)	O(83)		1.947(7)
Mn(5)	O(65)		1.912(7)	Mn(8)	O(89)		1.962(6)
Mn(5)	O(121)		2.242(7)	Mn(8)	O(137)		2.243(6)
Mn(6)	O(18)		1.899(7)	Mn(8)	O(138)		2.262(7)
Mn(6)	O(19)		1.872(6)	Mn(9)	O(21)		1.865(6)
Mn(6)	O(59)		1.957(7)	Mn(9)	O(22)		1.897(6)
Mn(6)	O(73)		1.945(7)	Mn(12)	O(115)		1.936(7)
Mn(6)	O(123)		2.233(7)	Mn(12)	O(139)		2.201(7)
Mn(6)	O(125)		2.190(7)	Mn(12)	O(140)		2.219(7)
O(13)	Mn(1)	O(14)	84.21(27)	O(14)	Mn(1)	O(18)	90.62(27)
O(13)	Mn(1)	O(16)	80.03(25)	O(14)	Mn(1)	O(25)	174.39(27)
O(13)	Mn(1)	O(17)	172.36(28)	O(16)	Mn(1)	O(17)	96.00(26)
O(13)	Mn(1)	O(18)	98.65(27)	O(16)	Mn(1)	O(18)	174.18(27)
O(13)	Mn(1)	O(25)	92.28(27)	O(16)	Mn(1)	O(25)	91.49(26)
O(14)	Mn(1)	O(16)	83.61(25)	O(17)	Mn(1)	O(18)	84.64(27)
O(14)	Mn(1)	O(17)	88.88(27)	O(17)	Mn(1)	O(25)	94.37(27)
O(18)	Mn(1)	O(25)	94.2(3)	O(14)	Mn(4)	O(16)	84.26(26)
O(13)	Mn(2)	O(14)	83.04(26)	O(14)	Mn(4)	O(23)	172.8(3)
O(13)	Mn(2)	O(15)	83.78(25)	O(14)	Mn(4)	O(24)	101.67(26)
O(13)	Mn(2)	O(19)	92.05(26)	O(15)	Mn(4)	O(16)	83.50(26)
O(13)	Mn(2)	O(20)	88.15(26)	O(15)	Mn(4)	O(23)	94.20(26)
O(13)	Mn(2)	O(33)	174.77(26)	O(15)	Mn(4)	O(24)	170.62(27)
O(14)	Mn(2)	O(15)	79.71(25)	O(15)	Mn(4)	O(49)	95.13(26)
O(14)	Mn(2)	O(19)	94.77(26)	O(16)	Mn(4)	O(23)	91.73(27)
O(14)	Mn(2)	O(20)	170.93(27)	O(16)	Mn(4)	O(24)	87.34(27)
O(14)	Mn(2)	O(33)	95.05(26)	O(16)	Mn(4)	O(49)	175.40(27)
O(15)	Mn(2)	O(19)	173.43(27)	O(23)	Mn(4)	O(24)	84.04(27)
O(15)	Mn(2)	O(20)	101.53(26)	O(23)	Mn(4)	O(49)	92.75(26)
O(15)	Mn(2)	O(33)	91.10(25)	O(24)	Mn(4)	O(49)	94.15(27)
O(19)	Mn(2)	O(20)	83.36(28)	O(17)	Mn(5)	O(18)	83.89(27)
O(19)	Mn(2)	O(33)	92.96(26)	O(17)	Mn(5)	O(27)	88.41(27)
O(20)	Mn(2)	O(33)	93.91(27)	O(17)	Mn(5)	O(57)	178.2(3)
O(13)	Mn(3)	O(15)	83.91(25)	O(17)	Mn(5)	O(65)	94.76(27)
O(13)	Mn(3)	O(16)	80.92(26)	O(17)	Mn(5)	O(121)	95.03(25)
O(13)	Mn(3)	O(21)	95.34(26)	O(18)	Mn(5)	O(27)	88.13(28)
O(13)	Mn(3)	O(22)	173.99(27)	O(18)	Mn(5)	O(57)	95.3(3)
O(13)	Mn(3)	O(41)	93.22(26)	O(18)	Mn(5)	O(65)	178.6(3)
O(15)	Mn(3)	O(16)	84.62(26)	O(18)	Mn(5)	O(121)	91.78(26)
O(15)	Mn(3)	O(21)	89.33(27)	O(27)	Mn(5)	O(57)	89.9(3)

Table 2 (Continued)

O(15)	Mn(3)	O(22)	90.08(25)	O(27)	Mn(5)	O(65)	92.25(28)
O(15)	Mn(3)	O(41)	176.33(25)	O(27)	Mn(5)	O(121)	176.53(25)
O(16)	Mn(3)	O(21)	173.18(27)	O(57)	Mn(5)	O(65)	86.1(3)
O(16)	Mn(3)	O(22)	98.72(27)	O(57)	Mn(5)	O(121)	86.61(28)
O(16)	Mn(3)	O(41)	92.68(26)	O(65)	Mn(5)	O(121)	87.92(26)
O(21)	Mn(3)	O(22)	84.40(26)	O(18)	Mn(6)	O(19)	93.50(26)
O(21)	Mn(3)	O(41)	93.22(27)	O(18)	Mn(6)	O(59)	92.5(3)
O(22)	Mn(3)	O(41)	92.78(26)	O(18)	Mn(6)	O(73)	175.1(3)
O(14)	Mn(4)	O(15)	79.46(25)	O(18)	Mn(6)	O(123)	93.48(28)
O(18)	Mn(6)	O(125)	93.7(3)	O(21)	Mn(8)	O(89)	90.37(27)
O(19)	Mn(6)	O(59)	173.8(3)	O(21)	Mn(8)	O(137)	93.78(25)
O(19)	Mn(6)	O(73)	90.62(27)	O(21)	Mn(8)	O(138)	86.03(26)
O(19)	Mn(6)	O(123)	88.96(26)	O(83)	Mn(8)	O(89)	83.04(28)
O(19)	Mn(6)	O(125)	92.57(27)	O(83)	Mn(8)	O(137)	91.09(27)
O(59)	Mn(6)	O(73)	83.4(3)	O(83)	Mn(8)	O(138)	88.53(28)
O(59)	Mn(6)	O(123)	92.18(28)	O(89)	Mn(8)	O(137)	86.39(25)
O(59)	Mn(6)	O(125)	85.5(3)	O(89)	Mn(8)	O(138)	88.70(25)
O(73)	Mn(6)	O(123)	83.87(27)	O(137)	Mn(8)	O(138)	175.09(24)
O(73)	Mn(6)	O(125)	88.8(3)	O(21)	Mn(9)	O(22)	84.44(26)
O(123)	Mn(6)	O(125)	172.52(28)	O(21)	Mn(9)	O(43)	89.06(26)
O(19)	Mn(7)	O(20)	82.82(26)	O(21)	Mn(9)	O(91)	92.99(27)
O(19)	Mn(7)	O(35)	88.86(26)	O(21)	Mn(9)	O(97)	179.4(3)
O(19)	Mn(7)	O(75)	95.1(3)	O(21)	Mn(9)	O(129)	89.00(25)
O(19)	Mn(7)	O(81)	178.06(27)	O(22)	Mn(9)	O(43)	87.80(25)
O(19)	Mn(7)	O(127)	91.28(27)	O(22)	Mn(9)	O(91)	176.53(26)
O(20)	Mn(7)	O(35)	86.68(26)	O(22)	Mn(9)	O(97)	95.97(26)
O(20)	Mn(7)	O(75)	175.8(3)	O(22)	Mn(9)	O(129)	91.27(24)
O(20)	Mn(7)	O(81)	95.73(27)	O(43)	Mn(9)	O(91)	94.50(25)
O(20)	Mn(7)	O(127)	93.4(3)	O(43)	Mn(9)	O(97)	90.50(26)
O(35)	Mn(7)	O(75)	89.7(3)	O(43)	Mn(9)	O(129)	177.92(24)
O(35)	Mn(7)	O(81)	92.35(26)	O(91)	Mn(9)	O(97)	86.61(27)
O(35)	Mn(7)	O(127)	179.85(28)	O(91)	Mn(9)	O(129)	86.35(25)
O(75)	Mn(7)	O(81)	86.5(3)	O(97)	Mn(9)	O(129)	91.44(25)
O(75)	Mn(7)	O(127)	90.2(3)	O(22)	Mn(10)	O(23)	93.93(26)
O(81)	Mn(7)	O(127)	87.52(27)	O(22)	Mn(10)	O(99)	93.35(26)
O(20)	Mn(8)	O(21)	93.82(27)	O(22)	Mn(10)	O(105)	176.21(26)
O(20)	Mn(8)	O(83)	93.07(28)	O(22)	Mn(10)	O(131)	96.51(26)
O(20)	Mn(8)	O(89)	174.84(28)	O(22)	Mn(10)	O(133)	91.04(26)
O(20)	Mn(8)	O(137)	90.31(25)	O(23)	Mn(10)	O(99)	172.1(3)
O(20)	Mn(8)	O(138)	94.60(26)	O(23)	Mn(10)	O(105)	89.85(27)
O(21)	Mn(8)	O(83)	171.5(3)	O(23)	Mn(10)	O(131)	92.25(25)
O(23)	Mn(10)	O(133)	91.33(25)	O(67)	Mn(12)	O(139)	93.01(26)
O(99)	Mn(10)	O(105)	82.85(27)	O(67)	Mn(12)	O(140)	84.5(3)
O(99)	Mn(10)	O(131)	89.93(26)	O(115)	Mn(12)	O(139)	83.6(3)
O(99)	Mn(10)	O(133)	85.51(26)	O(115)	Mn(12)	O(140)	88.1(3)
O(105)	Mn(10)	O(131)	83.57(25)	O(139)	Mn(12)	O(140)	171.5(3)
O(105)	Mn(10)	O(133)	88.63(27)	Mn(1)	O(13)	Mn(2)	95.23(28)
O(131)	Mn(10)	O(133)	171.40(25)	Mn(1)	O(13)	Mn(3)	99.72(27)
O(23)	Mn(11)	O(24)	81.69(26)	Mn(2)	O(13)	Mn(3)	94.75(27)
O(23)	Mn(11)	O(51)	88.16(25)	Mn(1)	O(14)	Mn(2)	95.7(3)
O(23)	Mn(11)	O(107)	94.86(26)	Mn(1)	O(14)	Mn(4)	95.96(27)
O(23)	Mn(11)	O(113)	176.6(3)	Mn(2)	O(14)	Mn(4)	100.54(27)
O(23)	Mn(11)	O(135)	89.36(25)	Mn(2)	O(15)	Mn(3)	95.89(27)
O(24)	Mn(11)	O(51)	85.73(25)	Mn(2)	O(15)	Mn(4)	100.22(27)
O(24)	Mn(11)	O(107)	174.69(27)	Mn(3)	O(15)	Mn(4)	94.61(26)
O(24)	Mn(11)	O(113)	96.86(27)	Mn(1)	O(16)	Mn(3)	99.3(3)
O(24)	Mn(11)	O(135)	93.02(26)	Mn(1)	O(16)	Mn(4)	94.29(26)
O(51)	Mn(11)	O(107)	90.14(26)	Mn(3)	O(16)	Mn(4)	95.65(27)
O(51)	Mn(11)	O(113)	94.77(27)	Mn(1)	O(17)	Mn(5)	94.8(3)
O(51)	Mn(11)	O(135)	177.37(25)	Mn(1)	O(17)	Mn(12)	133.2(3)
O(107)	Mn(11)	O(113)	86.80(28)	Mn(5)	O(17)	Mn(12)	131.6(3)
O(107)	Mn(11)	O(135)	90.97(27)	Mn(1)	O(18)	Mn(5)	93.8(3)
O(113)	Mn(11)	O(135)	87.68(27)	Mn(1)	O(18)	Mn(6)	132.2(3)
O(17)	Mn(12)	O(24)	93.65(26)	Mn(5)	O(18)	Mn(6)	123.8(3)
O(17)	Mn(12)	O(67)	90.53(27)	Mn(2)	O(19)	Mn(6)	134.5(4)
O(17)	Mn(12)	O(115)	173.54(27)	Mn(2)	O(19)	Mn(7)	96.3(3)
O(17)	Mn(12)	O(139)	96.11(26)	Mn(6)	O(19)	Mn(7)	126.6(3)
O(17)	Mn(12)	O(140)	92.0(3)	Mn(2)	O(20)	Mn(7)	94.85(26)
O(24)	Mn(12)	O(67)	175.31(28)	Mn(2)	O(20)	Mn(8)	130.6(3)
O(24)	Mn(12)	O(115)	92.80(27)	Mn(7)	O(20)	Mn(8)	127.1(4)
O(24)	Mn(12)	O(139)	88.65(25)	Mn(3)	O(21)	Mn(8)	132.0(3)
O(24)	Mn(12)	O(140)	93.26(27)	Mn(3)	O(21)	Mn(9)	95.4(3)
O(67)	Mn(12)	O(115)	83.04(28)	Mn(8)	O(21)	Mn(9)	132.3(3)
Mn(3)	O(22)	Mn(9)	93.19(26)	Mn(11)	O(135)	N(134)	122.5(6)
Mn(3)	O(22)	Mn(10)	131.6(3)	O(121)	N(122)	O(123)	119.8(8)

Table 2 (Continued)

Mn(9)	O(22)	Mn(10)	123.7(3)	O(121)	N(122)	O(124)	117.8(9)
Mn(4)	O(23)	Mn(10)	133.6(4)	O(123)	N(122)	O(124)	122.3(8)
Mn(4)	O(23)	Mn(11)	96.50(27)	O(125)	N(126)	O(127)	131.5(13)
Mn(10)	O(23)	Mn(11)	127.4(3)	O(125)	N(126)	O(128)	117.8(14)
Mn(4)	O(24)	Mn(11)	95.46(28)	O(127)	N(126)	O(128)	110.1(14)
Mn(4)	O(24)	Mn(12)	132.1(3)	O(129)	N(130)	O(131)	118.3(8)
Mn(11)	O(24)	Mn(12)	128.4(3)	O(129)	N(130)	O(132)	119.1(9)
Mn(5)	O(121)	N(122)	127.1(6)	O(131)	N(130)	O(132)	122.6(8)
Mn(6)	O(123)	N(122)	125.9(6)	O(133)	N(134)	O(135)	123.7(9)
Mn(6)	O(125)	N(126)	128.3(8)	O(133)	N(134)	O(136)	118.7(10)
Mn(7)	O(127)	N(126)	123.3(8)	O(135)	N(134)	O(136)	117.5(10)
Mn(9)	O(129)	N(130)	137.0(6)	O(143)	N(142)	O(144)	124.8(13)
Mn(10)	O(131)	N(130)	130.1(6)	O(143)	N(142)	C(141)	117.7(11)
Mn(10)	O(133)	N(134)	121.2(6)	O(144)	N(142)	C(141)	117.4(12)

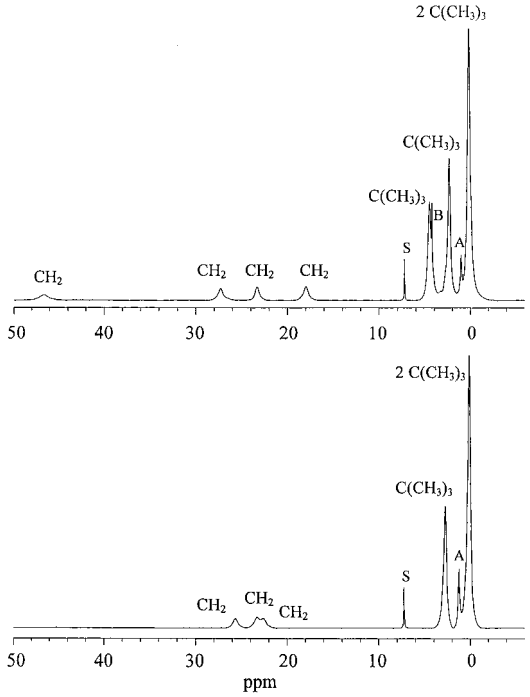

Figure 3. The ^{1}H NMR spectra in $CDCl_3$ at ~50 °C for $[Mn_{12}O_{12}(O_2CCH_2Bu^t)_{16}(H_2O)_4]$ (**3**) (top) and $[Mn_{12}O_{12}(NO_3)_4(O_2CCH_2Bu^t)_{12}(H_2O)_4]$ (**6**) (bottom). A = $Bu^tCH_2CO_2H$, B = $MeNO_2$, and S = $CHCl_3$.

Table 3. ^{1}H NMR Data[a] for $[Mn_{12}O_{12}(O_2CCH_2Bu^t)_{16}(H_2O)_4]$ (**3**) and $[Mn_{12}O_{12}(NO_3)_4(O_2CCH_2Bu^t)_{12}(H_2O)_4]$ (**6**)

group	**3**	**6**
CH_2 (ax, $Mn^{III}Mn^{III}$)	46.6	–
CH_2 (eq, $Mn^{III}Mn^{III}$)	27.3	25.6
CH_2 (eq, $Mn^{III}Mn^{III}$)	23.3	23.3
CH_2 (ax, $Mn^{III}Mn^{IV}$)	18.0	22.6
Bu^t(ax, $Mn^{III}Mn^{III}$)	4.54	–
Bu^t(ax, $Mn^{III}Mn^{IV}$)	2.38	2.76
Bu^t(eq, $Mn^{III}Mn^{III}$)[b]	0.27	0.15

[a] Chemical shifts in ppm at ~23 °C in CD_2Cl_2 using the δ scale (shifts downfield are positive). [b] Twice the integration value of the other Bu^t peaks.

resonances at 27.3 and 23.3 ppm are therefore assigned to the diastereotopic CH_2 hydrogen nuclei of the equatorial groups.

IR Spectroscopy. The IR spectrum of **6** displays the typical profile of a Mn_{12} complex in the 500−750 cm^{-1} region assigned to Mn−O stretches. The regions around 1550 and 1400 cm^{-1} exhibit the asymmetric and symmetric OCO stretches, respectively, of carboxylate ligands in their usual syn,syn bidentate bridging mode.[20] Comparison of the IR spectra of **3** and **6** indicates three bands at 1548, 1293, and 1047 cm^{-1} in the spectrum of **6** assignable to the NO_3^- groups.

The correlation between the structures and vibrational spectra of a large number of NO_3^- -containing metal complexes has been extensively investigated.[20] No pattern in the IR spectra has been identified that allows for unambiguous differentation of these structures, since the local symmetry of the NO_3^- group differs very little among the different binding modes. However, NO_3^- ligands usually have three main bands in the 1630−1485, 1160−1300, and 1050−960 cm^{-1} regions, and a large energy gap between the first two bands is usually indicative of bidentate coordination. The difference in energy between the highest wavenumber bands for **6** (255 cm^{-1}) can be considered large compared with literature examples and is consistent with a bidentate, bridging mode.

Magnetochemistry of Complex 6. Variable-temperature DC magnetic susceptibility (χ_M) data were collected in the 2.00−300 K range in a 10 kG (1 T) magnetic field. The $\chi_M T$ versus T behavior is similar to those of previously studied $[Mn_{12}O_{12}(O_2CR)_{16}(H_2O)_4]$ complexes,[1,3b] exhibiting a near temperature-independent value of 16−18 cm^3 K mol^{-1} in the 150−300 K range and then increasing rapidly to a maximum of ~47 cm^3 K mol^{-1} at ~20 K, before decreasing rapidly at lower temperatures. The maximum indicates a large ground state spin (S) value, and the low temperature decrease is primarily due to zero-field splitting effects.

$[Mn_{12}O_{12}(O_2CR)_{16}(H_2O)_4]$ complexes that have been well studied have S = 10 ground states. To characterize the ground state of complex **6**, magnetization (M) data were collected in the 10.0−70.0 kG field range and 1.80−25.0 K temperature range to complement the available 10 kG data. Shown in Figure 4 , is a plot of the data as reduced magnetization ($M/N\mu_B$) versus H/T, where N is Avogadro's number and μ_B is the Bohr magneton. For a system occupying only the ground state and experiencing no zero-field splitting (ZFS), the various isofield lines would be superimposed and $M/N\mu_B$ would saturate at a value of gS. The nonsuperimposition of the isofield lines clearly indicates the presence of ZFS. The data were fit assuming only the ground state is populated at these temperatures, using the methods described elsewhere involving diagonalization of the spin Hamiltonian matrix, incorporating axial ZFS (DS_z^2) and Zeeman interactions, and incorporating a full powder average of the magnetization.[21] The best fit is shown as solid lines in Figure 4, and the fitting parameters were S = 10, g = 1.92, and D = −0.40 cm^{-1} = −0.58 K. Thus, the replacement of four carboxylate groups with four NO_3^- groups does not change the ground state, a result consistent with the minimal structural perturbation of the core resulting from this substitution. The $[Mn_{12}O_{12}(O_2CR)_{16}(H_2O)_4]$ complexes show single-molecule magnetism behavior as a result of their S = 10 ground states,[1−3] and an investigation of whether **6** also retains these properties was therefore carried out.

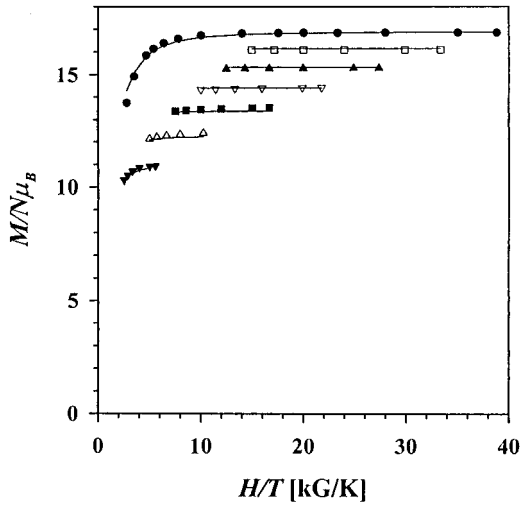

Figure 4. Plot of reduced magnetization ($M/N\mu_B$) versus H/T for $[Mn_{12}O_{12}(NO_3)_4(O_2CCH_2Bu^t)_{12}(H_2O)_4]\cdot H_2O$ (**6**·H_2O) at 10 (▼), 20 (△), 30 (■), 40 (▽), 50 (▲), 60 (□), and 70 (●) kG. The solid lines are fits using the appropriate method;[21] see the text for the fitting parameters.

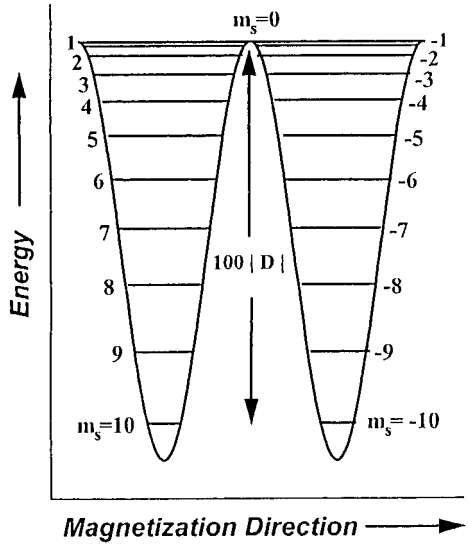

Figure 5. Double-well potential energy plot for a S = 10 molecule with axial symmetry and easy-axis type anisotropy. The energy separation between the $M_s = \pm 10$ and $M_s = 0$ orientations of the magnetization is given by $S^2|D|$.

AC Susceptibility Studies. In an AC susceptibility experiment, a weak field (typically 1−5 Oe) oscillating at a particular frequency (ν) is applied to a sample to probe the dynamics of its magnetization relaxation.[1,3] An out-of-phase AC susceptibility signal (χ_M'') is observed when the rate at which the magnetization (magnetic moment) of a molecule (or collection of molecules) relaxes (reorients) is close to the operating frequency of the AC field. Thus, if a collection of SMM's is maintained at a certain temperature and the frequency of the AC magnetic field is varied, a maximum in the χ_M'' signal will occur when the oscillation frequency of the field equals the rate at which a molecule can interconvert between the halves of the potential energy double well shown in Figure 5. This figure shows a plot of the potential energy of a S = 10 molecule exhibiting easy-axis type anisotropy (negative D value) as its magnetization (magnetic moment) vector changes from spin "up" ($M_s = -10$) to spin "down" ($M_s = +10$) via intermediate orientations. The potential energy barrier (U) is given by $U = S^2|D|$ for integer-spin systems. Frequency-dependent χ_M'' signals have been

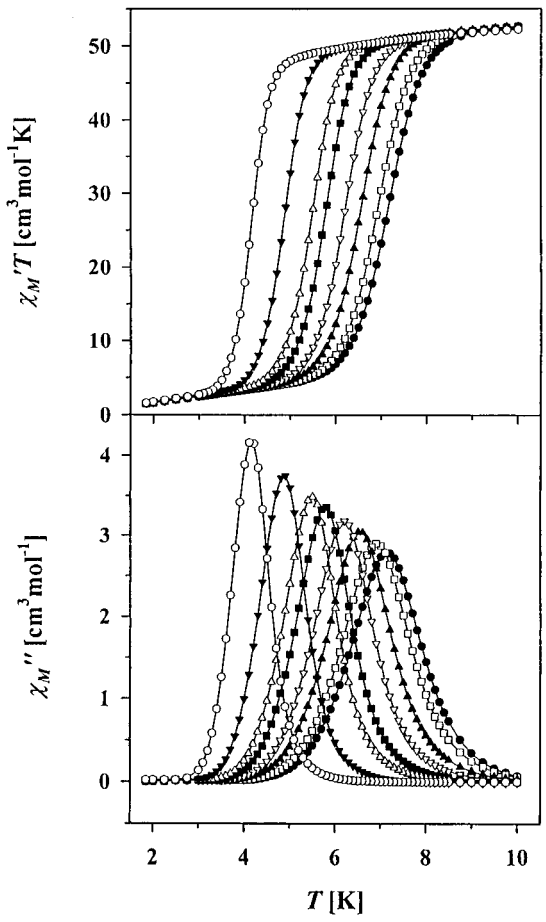

Figure 6. In-phase (χ_M') and out-of-phase (χ_M'') AC susceptibility signals for $[Mn_{12}O_{12}(NO_3)_4(O_2CCH_2Bu^t)_{12}(H_2O)_4]\cdot H_2O$ (**6**·H_2O) at 1 (○), 10 (▼), 50 (△), 100 (■), 250 (▽), 500 (▲), 1000 (□) and 1500 (●) Hz.

observed in the AC susceptibility studies of all Mn_{12} SMM's and are considered a diagnostic signature of the SMM property. In addition, AC magnetic susceptibility data can be employed to obtain the effective energy barrier (U_{eff}) for magnetization relaxation and even the spin of the ground state. For these reasons, AC susceptibility studies were performed on complex **6** to determine whether it retained the SMM behavior of its parent $[Mn_{12}O_{12}(O_2CR)_{16}(H_2O)_4]$ family.

The AC susceptibility of **6**·H_2O is shown in Figure 6 in a 3.5 Oe AC field oscillating at the indicated frequencies. The upper panel shows the $\chi_M'T$ versus T plot, where χ_M' is the in-phase magnetic susceptibility, and the lower panel shows the χ_M'' versus T plot. The frequency-dependent decrease in the $\chi_M'T$ versus T plot is a signature of the magnetization relaxation rate becoming comparable with the AC frequency. If so, a χ_M'' signal should appear at the corresponding temperatures, and the χ_M'' versus T plot shows that this is indeed the case; there are frequency-dependent χ_M'' signals in the 4−7 K range, which demonstrates that complex **6** is an SMM. Note that only one χ_M'' peak is seen at each frequency, and thus the sample does not contain the new phenomenon of Jahn−Teller isomerism identified recently, whereby some Mn_{12} molecules possess an orientation of one JT axis that is equatorial rather than axial (vis à vis the Mn_{12} disk) and which causes an increase in the relaxation rate and a corresponding χ_M'' peak in the 2−4 K region.[22,23] Also note that the $\chi_M'T$ value at its near plateau value in the 10 K region can be used to determine the ground state of **6**, assuming that only the ground state is significantly populated

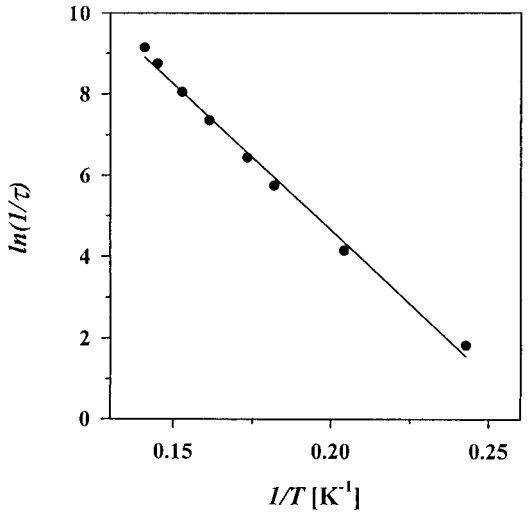

Figure 7. Plot of the natural logarithm of relaxation rate, $\ln(1/\tau)$ versus inverse temperature for $[Mn_{12}O_{12}(NO_3)_4(O_2CCH_2Bu^t)_{12}(H_2O)_4]\cdot H_2O$ (**6**·H_2O) using the χ_M'' versus T data of Figure 6. The solid line is a fit to the Arrhenius equation; see the test for the fitting parameters.

at these temperatures. The $\chi_M'T$ value of ~52 cm^3 $mol^{-1}K$ corresponds to an $S = 10$ system with $g = 1.94$, consistent with the reduced magnetization results above.

At the temperature of the χ_M'' versus T maximum, the relaxation rate equals the AC frequency (ν), and thus the relaxation rate ($1/\tau$) can be obtained from the relationship $\omega\tau = 1$, where $\omega = 2\pi\nu$. Thus, measurement of the peak maxima at several frequencies provides $1/\tau$ versus T data, and a kinetic analysis can be performed using the Arrhenius relationship (eqs 4a and 4b).

$$\frac{1}{\tau} = \frac{1}{\tau_0}\exp(-U_{eff}/kT) \tag{4a}$$

$$\ln(1/\tau) = -U_{eff}/kT + \ln(1/\tau_o) \tag{4b}$$

This is the characteristic behavior for a thermally activated Orbach process,[24,25] where U_{eff} is the effective anisotropy energy barrier, k is the Boltzmann constant, and T is the temperature. A plot of $\ln(1/\tau)$ versus $1/T$ using data collected at the eight AC frequencies of Figure 6 is given in Figure 7, with the least-squares fit to eq 4b shown as a solid line. From the slope and intercept were determined that $U_{eff} = 50.0$ $cm^{-1} = 72.0$ K and $1/\tau_0 = 1.9 \times 10^8$ s^{-1}. Similar results were obtained from multiple determinations, and on other versions of **6** that analyze with different solvation content (see Experimental Section).

The U_{eff} values for $[Mn_{12}O_{12}(O_2CR)_{16}(H_2O)_4]$ complexes are in the 42−45 cm^{-1} (60−65 K) range.[2,22,23,26]

Magnetization Hysteresis Loops. Since complex **6** has a sufficiently large barrier to magnetization reversal to show χ_M'' signals, it was of interest to investigate its magnetization response to a changing DC field. This experiment was performed using some small crystals of **6** that had been oriented with their easy axes parallel by exposing them to a 5.5 T field while in fluid eicosane and then allowing the eicosane to cool and solidify at room temperature, trapping the crystals of **6** in their parallel orientation.

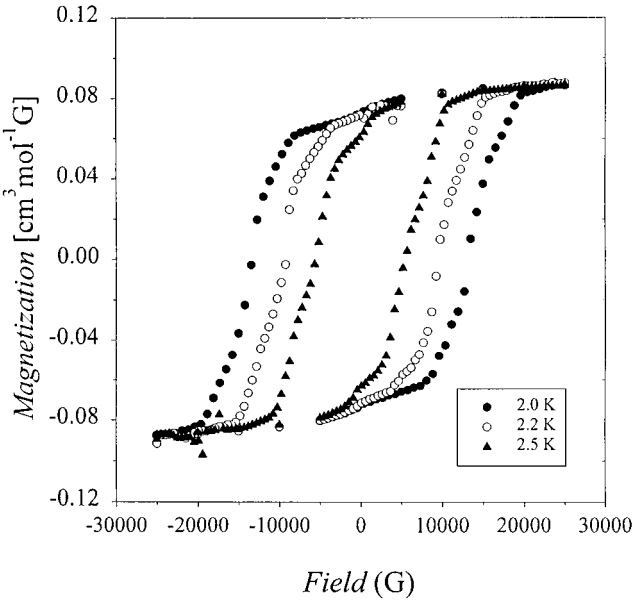

Figure 8. Hysteresis loops exhibited by complex **6** in magnetization versus applied field in the 2.0−2.5 K temperature range.

The magnetization versus DC field data measured for **6** are shown in Figure 8. Magnetization hysteresis loops are seen in the 2.0−2.5 K range. Thus, when a field of 2.5 T (25 kG) is employed, the magnetization of the molecules all line up parallel to the field (spin "up"), and a saturating magnetization is obtained. When the field is changed to zero, the magnetization does not decay to zero, as would be expected on rapid randomization of the magnetization direction, because there is a significant barrier (versus thermal energy at these temperatures) to magnetization reorientation. In zero applied field, the double-well potential energy plot of Figure 5 applies, with the molecules' magnetization all on one side of the double well ($M_s = -10$) as they are unable to overcome the barrier to reorientation. There is thus a remnant magnetization in the "up" direction. Reversal of the direction of the applied field (negative values in Figure 8) now makes the double well of Figure 5 asymmetric, lowering the barrier and allowing the molecules to reorient their magnetization to again be parallel to the field ($M_s = +10$; spin "down") until saturation is once more reached. Now when the field is changed to zero, a remnant magnetization in the "down" direction is obtained. The coercivity, or coercive field, required to change the remnant magnetization to zero is half the width of the hysteresis loop at the zero magnetization point, and it can be seen to increase with decreasing temperature, as expected.

Inspection of the magnetization hysteresis loops of Figure 8 shows, however, that the hysteresis loops are not smooth but instead show step features at regular intervals of applied field. Such steps were first seen on the hysteresis loops of $[Mn_{12}O_{12}(O_2CMe)_{16}(H_2O)_4]\cdot 2MeCO_2H\cdot 4H_2O$[12,13] and are due to quantum tunneling of the magnetization (QTM). Similar steps have since been seen on the hysteresis loops of other $[Mn_{12}O_{12}(O_2CR)_{16}(H_2O)_4]$ complexes,[3,5a,23] and for other complexes, such as $[Mn_4O_3Cl(O_2CMe)_3(dbm)_3]$ (dbm^- is the anion of dibenzoylmethane)[4] and $[Fe_8O_2(OH)_{12}(tacn)_6]^{8+}$ (tacn is 1,4,9-triazacyclononane).[8a] QTM can occur when a $-M_s$ state on one side of a symmetric or asymmetric potential energy double well is equienergetic with a $+M_s + n$ state (n = integer) on the other side. As a result, the magnetization can reverse from "spin up"

(24) van Duyneveldt, A. J. In *Magnetic Molecular Materials*; Gatteschi, D., Kahn, O., Miller, J., Palacio, F., Eds.; Kluwer Academic Publishers: London, 1991.
(25) Abragam, A.; Bleaney, B. *Electron Paramagnetic Resonance of Transition Ions*; Dover Press: Mineola, New York, 1986.
(26) Gatteschi, D.; Caneschi, A.; Pardi, L.; Sessoli, R. *Science* **1994**, *265*, 1054.

to "spin down" by tunneling through the anisotropy barrier rather than going over it. The first step is expected when the applied field is returned to zero after it has saturated the magnetization in a given direction ("spin up"). In zero field, the potential energy double well is symmetric (Figure 5), and all $-M_s$ states are degenerate with the corresponding $+M_s$ states, and QTM can occur. Reversal of the applied field results in the appearance of further steps at approximately regular intervals when $-M_s$ states are degenerate with $+M_s + n$ states in an asymmetric double well. Thus, the steps are evidence for field-tuned resonant tunneling of the magnetization. Complex **6** is thus exhibiting the same behavior demonstrated by the parent $[Mn_{12}O_{12}(O_2CR)_{16}(H_2O)_4]$ complexes.

The steps are regularly spaced in applied field and invariant with temperature (ignoring the small shift due to magnetic induction effects of dipolar fields from neighboring molecules in the crystal[12,27]). The field separation (ΔH) is related to D by eq 5.

$$\Delta H = \frac{|D|}{g\mu_B} \tag{5}$$

Measurement of the step positions in Figure 8 (using the first-derivative plot) gave an average ΔH of 0.449 T (= 4.49 kG), which gives $|D|/g = 0.21$ cm^{-1}. This may be compared with the $|D|/g$ value of 0.23 cm^{-1}, obtained from the HFEPR spectrum (see below), and 0.21 cm^{-1} obtained from the reduced magnetization fits. All three techniques thus give very similar values.

High-Frequency EPR (HFEPR) Spectroscopy. HFEPR measurements were made on complex **6** in order to provide additional characterization of the spin and anisotropy of the molecule, and to compare the obtained parameters with those for other Mn_{12} complexes studied previously. HFEPR is proving to be a very useful technique for the characterization of such molecular species with high anisotropy.[28−31] The observed transitions are between the M_s levels arising from zero-field splitting in the ground state, and an analysis of the resonance fields directly provides information on D. HFEPR spectra were recorded at 328.7 GHz at 30 K for an oriented microcrystalline sample of complex **6**·$^1/_2$Bu^{t}CH$_2$CO$_2$H. Figure 9 shows the 328.7 GHz spectrum taken at 30 K, and eight regularly spaced resonances are observed in the 0.5−10 T range. These resonances are due to transitions between zero-field split components of the S = 10 ground state of the complex, i.e., from the $M_s = -10$ to $M_s = -9$, $M_s = -9$ to $M_s = -8$, etc. In addition to the eight regularly spaced resonances, the fine structure contains some additional features. This is better seen in the bottom plot of Figure 9. Two resonances are seen as shoulders to the resonances at the low field edge. They are observed at ca. 1.0 and 2.5 T. The two shoulders appear to belong to a second fine structure pattern that overlaps the main parallel signals, perhaps from a fraction of sample that differs in solvent content. Additional resonances that make up the second fine structure pattern are not seen. At higher fields, the two sets of parallel signals overlap. This may be the origin for the rather broad parallel signals observed. The top plot in Figure 9 shows a sharp resonance at ca. 12.0 T in addition to the parallel signals. This is probably due to a trace amount of paramagnetic impurity contained in complex **6**, which is known to give a strong sharp signal near the $g = 2$ region.

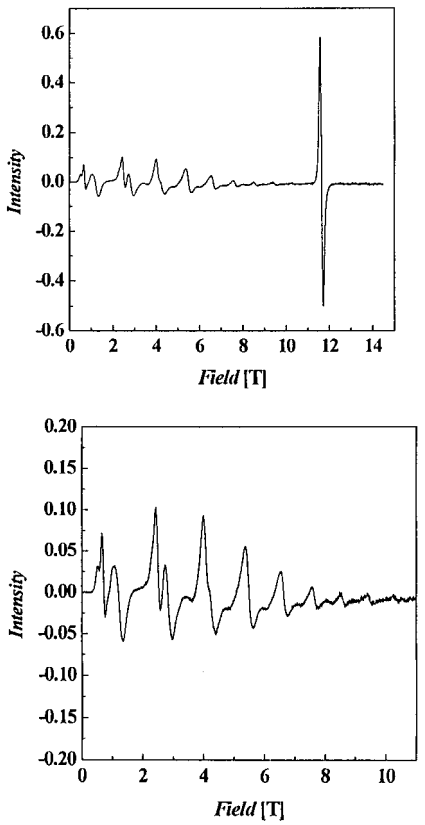

Figure 9. A 328.7 GHz HFEPR spectrum of complex **6** at 30 K. The top figure is the full spectrum from 0 to 14.5 T and bottom figure is an expanded view between 0 and 11 T.

Table 4. Resonance Fields in the HFEPR Spectrum[a] of $[Mn_{12}O_{12}(NO_3)_4(O_2CCH_2Bu^t)_{12}(H_2O)_4]\cdot{}^1/_2Bu^tCH_2CO_2H$

transition $M_s \rightarrow M_s + 1$	resonance exp	field (T) calc
−10 → −9	0.6641	0.7114
−9 → −8	2.4297	2.5176
−8 → −7	4.0029	3.9509
−7 → −6	5.3744	5.2409
−6 → −5	6.5443	6.5435
−5 → −4	7.5807	7.5894
−4 → −3	8.5147	8.5488
−3 → −2	9.4177	9.5475

[a] At 328.7 GHz and at 30 K.

The main parallel resonances shown in Figure 9 were analyzed to determine the anisotropy parameters of the ground state. The resonance fields are tabulated in Table 4 , and the data are plotted in Figure 10 as resonance field versus the M_s value for each $M_s \rightarrow (M_s + 1)$ transition. Table 4 and Figure 10 assume that the ground state is S = 10, and therefore, in a field, the lowest energy level has $M_s = -10$. Thus, at 328.7 GHz and 30 K, the $M_s = -10$ to $M_s = -9$ transition is seen at 0.66 T. From Figure 10, it is clear that the resonance field positions do not exhibit a linear dependency on M_s, i.e., the spacing between the parallel signals decreases with increasing fields. This shows that the spin Hamiltonian of eq 6, which includes only a second-order axial zero-field splitting term and would predict a linear dependence of the resonance field positions on M_s, is not applicable.

(27) Friedman, J. R.; Sarachik, M. P.; Tejada, J.; Maciejewski, J.; Ziolo, R. *J. Appl. Phys.* **1996**, *79*, 6031.
(28) Barra, A. L.; Caneschi, A.; Gatteschi, D.; Sessoli, R. *J. Am. Chem. Soc.* **1995**, *117*, 8855.
(29) Barra, A. L.; Caneschi, A.; Cornia, A.; Fabrizi de Biani, F.; Gatteschi, D.; Sangregorio, C.; Sessoli, R.; Sorace, L. *J. Am. Chem. Soc.* **1999**, *121*, 5302.
(30) Barra, A. L.; Gatteschi, D.; Sessoli, R. *Phys. Rev. B* **1997**, *56*, 8192.
(31) Barra, A. L.; Caneschi, A.; Gatteschi, D.; Sessoli, R. *J. Magn. Magn. Mater.* **1998**, *177−181*, 709.

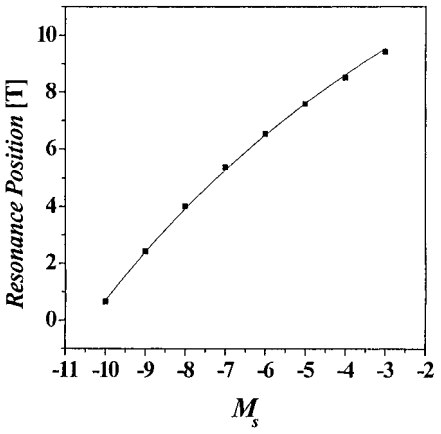

Figure 10. Least-squares fitting of the HFEPR data of Figure 9 to eq 8. See the text for the fitting parameters.

$$\hat{H} = g\mu_B \hat{H}\hat{S} + D\left[\hat{S}_z^2 - \frac{1}{3}S(S+1)\right] \quad (6)$$

To accommadate the non-linear behavior, the quartic zero-field interaction term $B_4^0\hat{O}_4^0$ was introduced into the spin Hamiltonian to give eq. 7,

$$\hat{H} = g\mu_B \hat{H}\hat{S} + D\left[\hat{S}_z^2 - \frac{1}{3}S(S+1)\right] + B_4^0\hat{O}_4^0 \quad (7)$$

where $\hat{O}_40 = 35S_z^4 - 30\ S(S+1)S_z^2 + 25S_z^2 + 6S(S+1)$. For an $S = 10$ system, this leads to eq 8 for the resonance field (H_r) for a parallel transition, where $D' = (3\cos^2\theta - 1)D/2g\mu_B$ and $B_4^{0\prime} = (3\cos^2\theta - 1)B_4^0/2g\mu_B$. The angle θ is the angle between the external magnetic field and the molecular z axis. Since the molecules of **6** in the crystal are canted 7.0° to each other, θ was taken as 3.5°. The resonance field data at 328.7 GHz were least-squares fit to eq 8 to give

$$H_r = g_e/g[H_0 - (2M_s + 1)(D' - 3275B_4^{0'}) - 35B_4^{0'}(4M_S^3 + 6M_S^2 + 4M_S + 1)] \quad (8)$$

where $g = 1.99$, $D = -0.46$ cm^{-1}, and $B_4^0 = -2.0 \times 10^{-5}$ cm^{-1}. The fit is shown as a solid line in Figure 10. The obtained value of B_4^0 for complex **6** is similar to the $B_4^0 = -2.2 \times 10^{-5}$ cm^{-1} determined for $[Mn_{12}O_{12}(O_2CMe)_{16}(H_2O)_4]$ (**1**). The $[Mn_4O_3Cl(O_2CMe)_3(dbm)_3]$ and $[Mn_4(O_2CMe)_2(pdmH)_6](ClO_4)_2\cdot 2.5H_2O$ SMM's have B_4^0 values of -7.8×10^{-5} and -2.0×10^{-5} cm^{-1}, respectively.[4c,6b]

Conclusions

Site-selective abstraction has been achieved for four carboxylate groups from $[Mn_{12}O_{12}(O_2CR)_{16}(H_2O)_4]$ complexes. The method relies on the presence of Mn^{III} Jahn−Teller elongation axes and the fact that these four carboxylate groups have both of their O atoms lying on JT axes, making them significantly more basic and thus more susceptible to electrophilic attack than the other twelve carboxylate groups. Stoichiometric nitric acid has proven to be the reagent of choice, causing loss of four carboxylate groups via protonation and providing NO_3^- groups to stabilize the carboxylate-depleted product. The crystal structure of complex **6** confirms that the NO_3^- groups are ordered at only four positions and that replacement of four carboxylate groups causes only minimal structural perturbation of the rest of the molecule. Consistent with this, a variety of magnetic and HFEPR studies demonstrate that complex **6** retains the $S = 10$ ground state of the parent $[Mn_{12}O_{12}(O_2CR)_{16}(H_2O)_4]$ complexes and a D value of -0.40 to -0.46 cm^{-1}, depending on the technique. Indeed, the consistency of the various obtained D values of **6** is satisfying, allowing for the differing assumptions and experimental errors inherent to different techniques. ^{1}H NMR studies confirm the solid-state structure of **6** is retained in solution. This augues well for the utility of **6** and **7** (and other carboxylate R group derivatives) as starting points for further chemistry. This could include attachment of other groups onto the Mn_{12} clusters at the NO_3^- positions by metathesis, taking advantage of the good leaving-group properties of this inorganic ion. The groups that could be attached need not be organic but instead suitably chosen metal-containing species, raising the possibility of controlled construction of assemblies of $[Mn_{12}]$ with other paramagnetic units. Such a system could provide the ability to modulate the spin (S) and other magnetically important properties of the ensemble (such as the anisotropy), allowing for improvement of single-molecule magnetism properties, as defined by slower magnetization relaxation rates and thus hysteresis loops at higher temperatures than for the Mn_{12} molecules, which are the best SMM's at present. In this regard, it was satisfying to discover that the NO_3^- -containing form of the $[Mn_{12}]$ complexes is not only stable in solution but retains the same $S = 10$ ground state and significantly large magnetoanisotropy of the $[Mn_{12}O_{12}(O_2CR)_{16}(H_2O)_4]$ and thus exhibits SMM properties essentially identical to those of the latter, i.e., the SMM properties are unperturbed by ligand alterations on the periphery of the molecule. This is important for the use of these molecules in future studies.

Acknowledgment. This work was supported by NSF Grants to G.C. and D.N.H.

Supporting Information Available: X-ray crystallographic files in CIF format for $[Mn_{12}O_{12}(NO_3)_4(O_2CCH_2Bu^t)_{12}(H_2O)_4]\cdot MeNO_2$. This material is available free of charge via the Internet at http://pubs.acs.org.

IC010252G